EUROFUSION WPJET1-PR(16) 15833

S Kwak et al.

Bayesian electron density inference using Gaussian processes from the JET Li-BES data

Preprint of Paper to be submitted for publication in Nuclear Fusion

This work has been carried out within the framework of the EUROfusion Consortium and has received funding from the Euratom research and training programme 2014-2018 under grant agreement No 633053. The views and opinions expressed herein do not necessarily reflect those of the European Commission.

Bayesian electron density inference using Gaussian processes from the JET Li-BES data

Sehyun Kwak[1,2†], J. Svensson[2], M. Brix[3], Y.-c. Ghim[1*], and JET Contributors‡

EUROfusion Consortium, JET, Culham Science Centre, Abingdon, OX14 3DB, UK
[1] Department of Nuclear and Quantum Engineering, KAIST, Daejeon 34141, Korea
[2] Max-Planck-Institut für Plasmaphysik, 17491 Greifswald, Germany
[3] Culham Centre for Fusion Energy, Culham Science Centre, Abingdon OX14 3DB, UK

E-mail: †slayer313@kaist.ac.kr, *ycghim@kaist.ac.kr

7 April 2016

Abstract. A Bayesian model to infer edge electron density profiles is developed for the JET lithium beam emission spectroscopy (Li-BES) system, measuring Li I (2p-2s) line radiation, consisting of 26 channels with $\sim$ 1 cm spatial resolution and $\sim$ 15 ms temporal resolution. The density profile is modelled through Gaussian processes with the hyperparameters governing their overall scale and scale length and sampled via Markov Chain Monte Carlo (MCMC) method from the inferred Li I line intensities expressed as a function of the plasma density by the multi-state model which describes all the processes between neutral lithium beam atoms and plasma particles. The line intensities are inferred based on the spectral model consistent with the measured spectra within their uncertainties including electrical fluctuations and photon statistics, where the spectral model takes into account of instrumental and interference filter functions estimated by separate measurements. Our newly developed method to infer profiles of edge electron density has following advantages: i) all the possible edge electron density profiles consistent with measured data are estimated, ii) the available radial range for density profiles is increased to the full observation range ($\sim$ 26 cm), iii) an assumption of monotonic electron density profile is not necessary, and iv) absolute calibration factor of the diagnostic system is automatically estimated overcoming the limitation of the conventional technique and allowing us to infer the electron density profiles for all pulses without preprocessing the data or an inner boundary assumption.

Keywords: Bayesian inference, Forward modelling, Gaussian process, Plasma diagnostics

Submitted to: *Nucl. Fusion*

‡ See the Appendix of F. Romanelli et al., Proceedings of the 25th IAEA Fusion Energy Conference 2014, Saint Petersburg, Russia

1. Introduction

Edge electron density profiles have been recognized as one of the key physical quantities for controlling and understanding edge plasma phenomena in magnetic confinement devices such as edge localised modes (ELMs) [1], L-H transitions [2] and turbulence transport [3]. Lithium beam emission spectroscopy (Li-BES) systems capable of providing the profiles of edge electron density, thus, have been widely used at various devices (TEXTOR [4, 5], ASDEX Upgrade [6, 7], W7-AS [6], and JET [8, 9, 10]). Li-BES system is a type of beam diagnostics that injects a neutral lithium beam into the plasma and measures the Li I (2p-2s) line radiation caused by spontaneous emission processes from the first excited state (1s2 2p1) to the ground state (1s2 2s1) of the neutral lithium beam atoms. The Li I line intensity can be expressed as a function of the plasma density by the multi-state model [11] which describes all the processes between lithium atoms and plasma particles. Therefore the profiles of edge electron density can be inferred from the measured profiles of the Li I line intensity.

The integral expression of the multi-state model which calculates a profile of electron density [4] from the measured Li-BES data has been used conventionally at many devices [5, 6, 8, 9]. This method, however, has a limitation that profiles of absolute electron density (based on the absolute calibration factor) can be obtained only if either a *singular point* of electron density is found or an inner boundary condition is provided in the data. Consequently, this method involves some weakness: i) a preprocessing of the data is usually required to find the singular point, ii) the singular point cannot be found accurately, iii) an infinitesimal change of the singular point can cause huge difference of the density profile and iv) an inner boundary, which is required if the singular point does not exist, cannot be properly fixed because it is almost impossible to obtain all the populations of the different states of the neutral Li beam atoms. Another method utilising Bayesian probability theory to analyse the Li-BES data was reported at ASDEX Upgrade [7] and made impressive progress. On the other hand, as they have made an assumption of monotonic density profile using a regularisation technique to reduce the possibility of obtaining non-monotonic profiles, the results may well clash with possibly actualised non-monotonic profiles agreeing with the data.

We claim that the proposed Bayesian inference method in this paper solves limitations of the above mentioned two existing methods. The proposed method requires neither preprocessing of the data, inner boundary information nor a monotonic profile assumption. Our proposed method improves profiles of edge electron both qualitatively and quantitatively.

Our proposed method basically comprises two parts. The first part is obtaining the profile of Li I line intensity. As the JET Li-BES system obtains spectral measurements, the raw data contains instrumental function, interference filter function, the intensities of Li I line radiation and backgrounds and the electronic offset as well as photon and electronic noises. We infer instrumental and interference filter functions based on separate measurements (which are required only once in a while as they do not

vary much shot-to-shot base) using Gaussian process based prior. We use Gaussian process because we do not know the parametric form, i.e., analytical expression of the functions. With these functions, we infer intensities of Li I line radiation and background and the electronic offset simultaneously. This provides an advantage of removing the necessity of beam modulations to obtain separate background measurements within a plasma shot. Furthermore, as the background intensity is likely to be dominated by Bremsstrahlung radiation, our method opens a possibility to obtain the effective charge Z_{eff} of plasmas. The second part of our method infers the profile of edge electron density based on the intensity profile of Li I line radiation using the multi-state mode. During this second part, we let the absolute calibration factor of the system to be inferred as well based on the measured data allowing us not to use the singular-point method mentioned above. Gaussian process based prior for the electron density profile is obtained based on the existing profiles accumulated over many years of JET experiments. All the data analyses here are performed based on Bayesian scheme within the Minerva framework [12], therefore the best estimation (maximum a posterior) of the profile and the uncertainties are inferred simultaneously consistent with the measured data.

This paper consists of two main sections and the conclusion. Sec. 2 describes the models we use: multi-state model describing how one can obtain electron density information from the Li I line radiation intensity, spectral model of our measured raw data and the forward model of the JET Li-BES system describing how the output of the diagnostic system can be translated into the photon counts. Sec. 3 explains how interference filter and instrumental functions are inferred, procedure of obtaining intensity of Li I line radiation and electron density profile. The conclusion is presented in Sec. 4.

2. Models

2.1. Physics based multi-state model

Li-BES system measures the intensities of the Li I (2p-2s) line radiation from the neutral lithium beam penetrating into the plasma. The Li I line radiation is produced by spontaneous emission processes from the first excited state (1s2 2p1) to the ground state (1s2 2s1) of the neutral lithium beam atoms. The Li I line intensity is a function of the population of the first excited state which can be expressed in terms of the plasma density via the multi-state model.

The simplified expression of the multi-state model or the collisional-radiative model [4] is

$$\frac{dN_i\left(t\right)}{dt} = \sum_{j=1}^{M_{\text{Li}}} \left[\sum_s n_s a_{ij}^s \left(v_r^s\right) + b_{ij} \right] N_j, \tag{1}$$

which describes population and de-population of all the states of the neutral lithium atoms caused by all the processes between lithium beam atoms and plasma particles in addition to spontaneous emissions. N_i is the *relative* population of the i^{th} state

with respect to the total number of the neutral lithium beam atoms at the position where the lithium beam enters a tokamak vacuum vessel. For instance, $N_1 = 0.7$ and $N_2 = 0.1$ mean that 70 % and 10 % of the initial neutral lithium beam atoms are in the ground and first excited states, respectively. M_{Li} is the number of states of the neutral lithium atoms, and we consider nine different states in this paper; thus, $M_{\mathrm{Li}} = 9$. n_s is the plasma density of species s where $s = e$ and $s = p$ denote electron and proton, respectively. $a^s_{ij}\,(i \neq j) > 0$ is a net population rate coefficient by the plasma species s from the j^{th} state to the i^{th} state increasing the relative population of the i^{th} state, while $a^s_{ii} < 0$ is a net de-population rate coefficients including excitation, de-excitation and ionization effects leaving the i^{th} state. All population and de-population rate coefficients caused by plasma species s depend on the relative speed between the neutral lithium beam atoms and plasma species s which is denoted as v^s_r. b_{ij} is the spontaneous emission rate coefficient or Einstein coefficient.

It becomes easier to solve Eq. (1) if it is expressed in terms of the beam coordinate z: $d/dt = dz/dt \cdot d/dz$. Realising that dz/dt is the velocity of neutral lithium beam atoms v_{Li}, we obtain

$$\frac{dN_i\,(z)}{dz} = \frac{1}{v_{\mathrm{Li}}} \sum_{j=1}^{M_{\mathrm{Li}}} \left[\sum_s n_s\,(z)\, a^s_{ij}\,(v^s_r\,(z)) + b_{ij} \right] N_j\,(z)\,. \tag{2}$$

Here, we assume that v_{Li} is constant over the penetration range of the beam into plasmas.

The relative speed $v^s_r\,(z)$ is not directly measured but can be approximated using other quantities. The relative speed between neutral lithium beam atoms and electrons $v^e_r\,(z)$ is dominated by the electron temperature T_e since the typical (thermal) speed of electrons is much faster than the neutral lithium beam atoms. The relative speed between neutral lithium beam atoms and protons $v^p_r\,(z)$ can be approximated to the lithium beam velocity in case of JET Li-BES since the lithium beam energy is ~ 55 keV which is much higher than the ion temperature. Other species are not considered in this work. Thus, the multi-state model becomes

$$\frac{dN_i\,(z)}{dz} = \frac{1}{v_{\mathrm{Li}}} \sum_{j=1}^{M_{\mathrm{Li}}} \left[n_e\,(z)\, a^e_{ij}\,(T_e\,(z)) + n_p\,(z)\, a^p_{ij}\,(v_{\mathrm{Li}}) + b_{ij} \right] N_j\,(z)\,, \tag{3}$$

$$N_i\,(z = 0) = \delta_{1i}, \tag{4}$$

with the initial condition Eq. (4) where we assume that all the lithium beam atoms are neutral and in the ground state ($i = 1$) at the initial position where the beam enters the tokamak vacuum vessel corresponding to $z = 0$, i.e., $N_1\,(z = 0) = 1$. All the rate coefficients have been obtained from the Atomic Data Analysis Structure (ADAS) [13] and the reference [14]. Fig. 1 shows an example of steady-state relative populations for the first excited state N_2 as a function of electron density and temperature with the beam energy of 50 keV.

Note that this multi-state model does not consider the population of the ionised lithium atoms as the ionised ones *leave* the beam coordinate due to the strong magnetic field of JET. Therefore, electron loss processes such as ionization and charge-

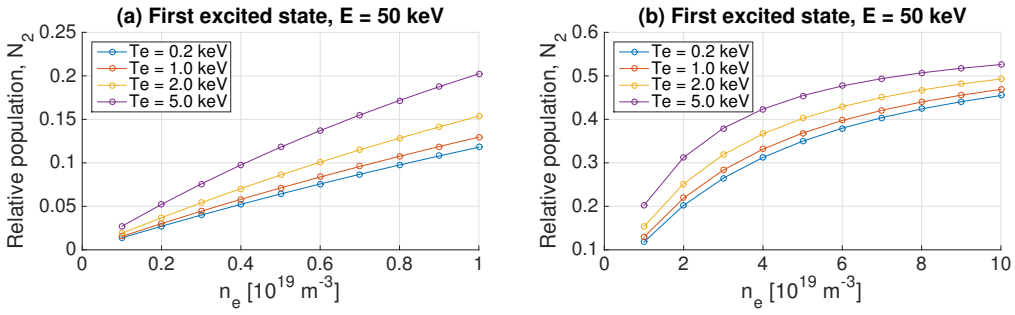

Figure 1. Steady-state relative populations of the first excited state (N_2) of the neutral lithium beam atoms as a function of the electron density and temperature with the beam energy of 50 keV in the range of (a) $0.1 \times 10^{19} < n_e < 1.0 \times 10^{19}$ and (b) $1.0 \times 10^{19} < n_e < 10.0 \times 10^{19}$.

exchange simply attenuate the total population of neutral lithium beam atoms, i.e., $\sum_{j=1}^{M_{\mathrm{Li}}} N_j\left(z>0\right)<1$.

2.2. Spectral model

The JET Li-BES system measures the spectra covering a few nanometres in wavelength including the Doppler shifted Li I line radiation from the 26 different spatial positions. A charge coupled device (CCD) camera detects the photons with approximately 10 ms integration time to increase the photon counts. More detailed description of the JET Li-BES system can be found elsewhere [9, 10].

A spectrum for each spatial position contains three types of signals (in addition to noise): i) lines caused by processes between impurities and plasmas, i.e., impurity line radiation, as well as Li I line radiation, ii) a background dominated by Bremsstrahlung radiation and iii) an electronic offset. A Doppler broadening of the Li I line radiation is negligible since the lithium beam is a mono-energetic beam ($\sim$ 0.02 nm broadening occurs for the beam temperature of $\sim$ 10 eV, and the dispersion of the CCD pixel is $\sim$ 0.04nm/pixel), therefore we treat the Li I line as a delta function in a spectrum. A measured spectrum $S\left(\lambda\right)$ from each spatial position can be expressed as

$$S\left(\lambda\right)=D\left(\lambda\right)\left[C\left(\lambda\right)A+B\right]+Z, \tag{5}$$

where A is the intensity of Li I line radiation, B the background level and Z the electronic offset which are inferred through Bayesian scheme with their uncertainties in a consistent way. The instrumental function $C\left(\lambda\right)$ and interference filter function $D\left(\lambda\right)$ are inferred through Bayesian scheme with Gaussian processes from the separate measurement [15]. Here, λ is the wavelength which has a one-to-one correspondence with the CCD pixel index [9].

Gaussian process, a set of possible variables associated with a multivariate Gaussian distribution, is one of the non-parametric models [16] and introduced here to infer $C\left(\lambda\right)$ and $D\left(\lambda\right)$ in a non-parametric way since their parametric forms are unknown. Their

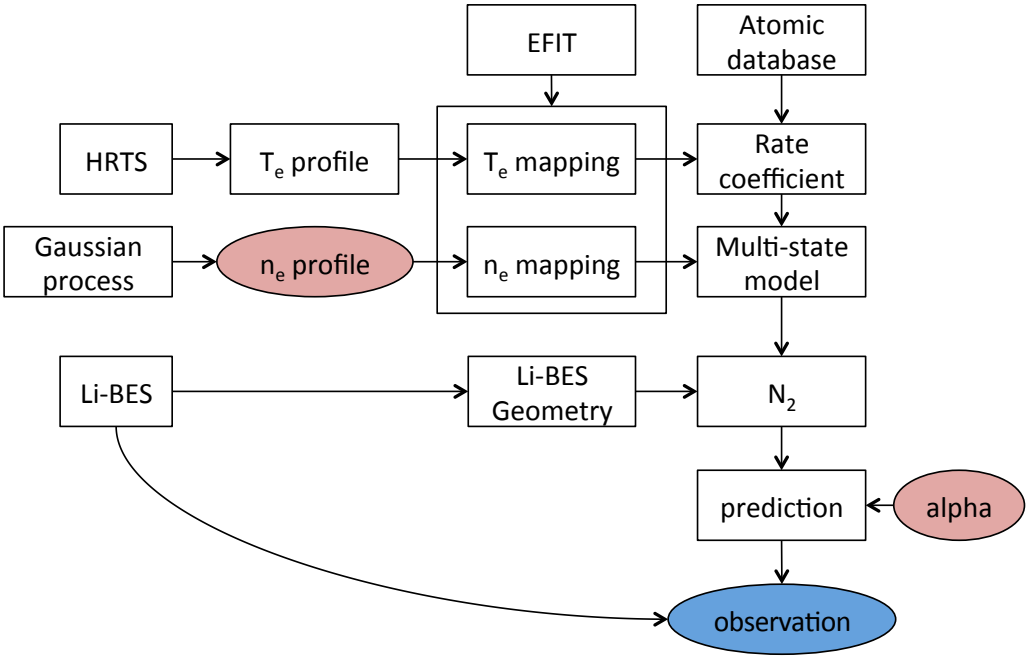

Figure 2. A simplified graphical representation of the JET Li-BES forward model implemented in Minerva [12]. The free parameters are shown with red circles; whereas values of parameters in the rectangles are either given or can be estimated once the free parameters are chosen. The electron density n_e and temperature T_e are mapped onto the EFIT estimated normalised flux surface. The relative populations of the neutral lithium beam atoms are analytically calculated from the multi-state model, and profiles of the Li I line radiation intensity are predicted given edge n_e profiles and absolute calibration factor, alpha (α). All the possible edge n_e profiles whose predicted Li I line intensity profile agree with the observation (blue circle) within their uncertainties are found.

hyperparameters are selected based on the measurements by maximising the *evidence* through Bayesian model selection. A detailed description of the Bayesian inference and modelling of the JET Li-BES data with Gaussian process can be found elsewhere [15].

2.3. Forward model

Our goal basically is to find all the possible profiles of the edge electron density n_e consistent with the observation, i.e., measured data from the JET Li-BES system. For this, we consider a forward model as shown in Fig. 2.

We start from a profile of edge electron density n_e, which is a set of free parameters, formed by Gaussian process with the hyperparameters, their overall scale and scale

length, which is discussed in more detail in Sec. 3.3. Edge n_e profiles are mapped onto the normalised flux surface coordinate ψ calculated by the EFIT, one of the equilibrium solvers. The electron temperature T_e, required for the rate coefficients a^s_{ij}, is measured by the High Resolution Thomson Scattering (HRTS) system [17] and mapped onto the same flux surface coordinate. This will allow us to calculate the relative population of the first excited state of the neutral lithium beam atoms, i.e., N_2, based on the multi-state model Eq. (3) with a quasi-neutrality condition, i.e., $n_e = n_p$. Here, we assume that impurity densities are low enough to be ignored§.

Once we have N_2, we can predict the Li I line radiation intensity, A in Eq. (5), where the detailed procedure is provided in Sec. 2.3.1. Our forward model which provides the probability of observing (or measuring) a certain intensity of Li I line radiation, which we denote as $A^{\rm obs}$, given A which is a function of two free parameters n_e and absolute calibration factor α is

$$p\left(A^{\rm obs}|A\left(n_e,\alpha\right)\right) = \frac{1}{\sqrt{2\pi}\sigma}\exp -\frac{\left(A^{\rm obs}-A\left(n_e,\alpha\right)\right)^2}{2\sigma^2}, \tag{6}$$

where σ is the uncertainty associated with our observation $A^{\rm obs}$. This is our basic form of the forward model in this paper and is the *likelihood* within Bayes formula. We assume that deviations of the observation from the prediction has a Gaussian distribution. We discuss how we estimate σ and rationale to form a Gaussian distributed deviations in Sec. 2.3.2.

2.3.1. Detected number of photons for a forward model The Li I line intensity, A in Eq. (5), is proportional to the relative population of the first excited state N_2, i.e., $A \propto b_{12}N_2$ where b_{12} is the spontaneous emission rate coefficient from the first state to the ground state. The change of the relative population of the first excited state due to the spontaneous emission denoted as $|\Delta N_2|$ is

$$|\Delta N_2\left(z\right)| = \frac{|b_{12}|}{v_{\rm Li}}\Delta z\ N_2\left(z\right), \tag{7}$$

where Δz is the observation length. Since one spontaneous emission produces one photon, the total number of populated photons $N^{\rm pop}_{\rm ph}$ corresponding to Li I line radiation over the integration time Δt with the lithium beam current $I_{\rm Li}$ is

$$N^{\rm pop}_{\rm ph}\left(z\right) = I_{\rm Li}\Delta t\left|\Delta N_2\left(z\right)\right| = I_{\rm Li}\Delta t\frac{|b_{12}|}{v_{\rm Li}}\Delta z\ N_2\left(z\right). \tag{8}$$

The emitted photons falling into the solid angle of the collection optics pass through various mirrors, lens and grism before detected by the CCD camera. We denote all these effects of optics including the solid angle as an effective transmittance of the system T. Then, the number of photons detected by (or arrived to) the CCD camera $N^{\rm det}_{\rm ph}\left(z\right)$ is

$$N^{\rm det}_{\rm ph}\left(z\right) = TN^{\rm pop}_{\rm ph}\left(z\right) = TI_{\rm Li}\Delta t\frac{|b_{12}|}{v_{\rm Li}}\Delta z\ N_2\left(z\right). \tag{9}$$

§ If impurities are non-negligible, then our measured spectra may show strong impurity line radiation in which case we know that our assumption is not valid.

Also, we define Q as the count per photon of the CCD camera. Note that Q is not a quantum efficiency of the CCD camera, rather it simply describes the count produced by the CCD camera as an output when one photon is arrived to the CCD detector. Then, the CCD output count due to the Li I line radiation $N_{\mathrm{CCD}}^{\mathrm{Li}}$ which we measure is

$$\begin{aligned} N_{\mathrm{CCD}}^{\mathrm{Li}}(z) &= QN_{\mathrm{ph}}^{\mathrm{det}}(z) = QTI_{\mathrm{Li}}\Delta t\frac{|b_{12}|}{v_{\mathrm{Li}}}\Delta z N_2(z) \\ &= A(z)\int D(\lambda)\,C(\lambda)\,d\lambda, \end{aligned} \tag{10}$$

and this is, by definition, equal to the Li I line intensity A multiplied by the spectrally integrated signal of the instrumental function $C(\lambda)$ and the interference filter function $D(\lambda)$ in Eq. (5).

We finally obtain

$$A(z) = \underbrace{\frac{QTI_{\mathrm{Li}}\Delta t\frac{|b_{12}|}{v_{\mathrm{Li}}}\Delta z}{\int D(\lambda)\,C(\lambda)\,d\lambda}}_{\equiv\alpha} N_2(z) = \alpha N_2(z), \tag{11}$$

where α is the absolute calibration factor which is another free parameter in our forward model in addition to n_e profile as shown in Fig. 2. Note that relative calibration factors between the channels are encompassed within the instrumental function $C(\lambda)$.

2.3.2. Uncertainties for a forward model There exists unknowns or uncertainties in our measurements due to a theoretically irreducible level of uncertainty from the photon statistics following a Poisson distribution which has a property of equal mean and variance. Furthermore, we have additional noise source as a result of electrical fluctuations of the electronics which we choose as a Gaussian distribution, which has the maximum entropy when the measured mean and variance of the electrical fluctuations are given in our model.

To be able to determine a photon noise level, it is necessary to find the value of Q in Eq. (10) so that the measured $N_{\mathrm{CCD}}^{\mathrm{Li}}$ can be converted to the detected number of photons $N_{\mathrm{ph}}^{\mathrm{det}}$ which is the quantity following a Poisson distribution. With an aim of determining the value of Q, we shine a uniform intensity light emission diode (LED) to the CCD camera while varying the intensity of the LED with all other conditions fixed as if it were actual measurements of the Li-BES during plasma discharges. The arithmetic mean of CCD output counts $\bar{N}_{\mathrm{CCD}}$ and its associated variance σ_{CCD}^2 are

$$\bar{N}_{\mathrm{CCD}} = Q\bar{N}_{\mathrm{ph}} + \bar{N}_{\mathrm{CCD}}^{\mathrm{DC}} + \bar{Z}_{\mathrm{CCD}}, \tag{12}$$

$$\sigma_{\mathrm{CCD}}^2 = Q^2\sigma_{\mathrm{ph}}^2 + \sigma_{\mathrm{e}}^2 \tag{13}$$

where $\bar{N}_{\mathrm{ph}}$ is the mean of the number of photons detected by (arrived to) the CCD camera and $\bar{N}_{\mathrm{CCD}}^{\mathrm{DC}}$ the mean CCD output counts due to the dark current of the CCD. Here, $\bar{Z}_{\mathrm{CCD}}$ is the mean CCD offset. σ_{ph}^2 and σ_{e}^2 are the variances due to photon and electronic noises, respectively. Note that we treat fluctuations in the dark current as a part of the electronic noise because they exist in the absence of detected photons.

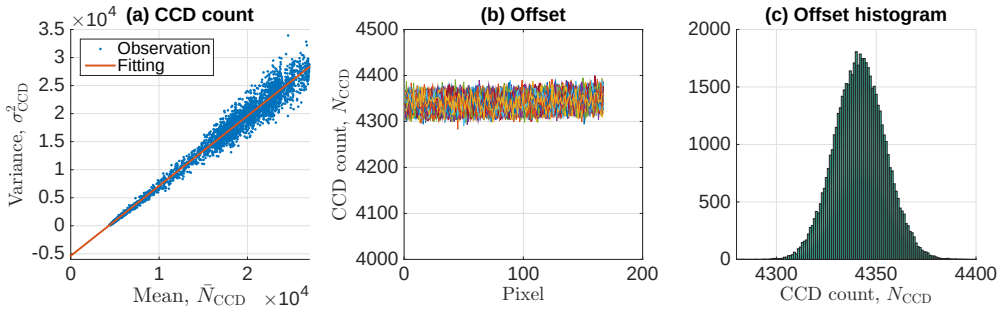

Figure 3. (a) The variance $\sigma^2_{\rm CCD}$ vs. the mean counts $\bar{N}_{\rm CCD}$ of the CCD output with varying LED intensities. The slope of the fitted linear line is the value of Q which is 1.247 ± 0.005. (b) Measurement of the CCD output counts as a function of the CCD pixel with all the electronics switched on and no input photons to the CCD, and (c) the histogram of the CCD output counts from (b). The histogram shows that i) the variance is 160, i.e., $\sigma^2_{\rm e} \approx 160$, with the mean value of 4342 and ii) it has a Gaussian shape.

Since we express the electronic noise as a Gaussian distribution, validity of Gaussian distributed fluctuations for the dark current can be questioned. We show that it is indeed valid shortly.

With $\bar{N}_{\rm ph} = \left(\bar{N}_{\rm CCD} - \bar{N}^{\rm DC}_{\rm CCD} - \bar{Z}_{\rm CCD}\right)/Q$ from Eq. (12) and $\bar{N}_{\rm ph} = \sigma^2_{\rm ph}$ owing to a Poisson distribution, Recasting Eq. (13), we get

$$\sigma^2_{\rm CCD} = Q\bar{N}_{\rm CCD} - (Q\bar{N}^{\rm DC}_{\rm CCD} + Q\bar{Z}_{\rm CCD} - \sigma^2_{\rm e}). \tag{14}$$

Notice that $\bar{N}_{\rm CCD}$ and $\sigma^2_{\rm CCD}$ can be directly measured with the LED on, and by varying the intensity of the LED we can determine the value of Q. Fig. 3(a) shows a graph of the measured $\sigma^2_{\rm CCD}$ vs. $\bar{N}_{\rm CCD}$ using the total of 4,175 (167 pixels from 25 channels) independent data points, the means and variances which are estimated using independent 332 time points. The slope is the value of Q we seek, and we find that $Q = 1.247 \pm 0.005$.

Now, we turn our attention to find the electronic fluctuation level $\sigma^2_{\rm e}$. This is simple: we switch on all the electronics and measure fluctuations in $N_{\rm CCD}$ without any photons to the CCD, i.e., $N_{\rm ph} = 0$. Here, $N_{\rm CCD}$ and $N_{\rm ph}$ are individual measurements rather than their means. Fig. 3(b) shows such measurements for all 26 spatial channels (different colours). Fig. 3(c) is the histogram of the $N_{\rm CCD}$. We estimate the variance to be 160 with the mean of 4342. Therefore, $\sigma^2_{\rm e} \approx 160$. As this measurement inevitably includes dark current noise, we argue that including dark current fluctuations in the electronic noise as a Gaussian distribution is valid as the histogram follows a Gaussian distribution. Furthermore, as we find the mean value of the offset, i.e., 4342, appears constantly for all channels, we always subtract this offset value from the measured signal before performing any analyses on the data. Any residual offset is captured by Z in Eq. (5).

A Poisson distribution with a large mean and variance can be approximated as a Gaussian distribution. Since the detected number of photons $N^{\rm det}_{\rm ph}$ is larger than 100, we

take the photon statistics follow a Gaussian distribution as well. Therefore, the variance σ^2 in Eq. (6) is

$$\sigma^2 = \sigma^2_{\rm ph} + \sigma^2_{\rm e}. \tag{15}$$

3. Bayesian inference

Inference on free parameters is a process to find possible values of the free parameters consistent with the available measured data. For our case, we have a measured spectrum $S(\lambda)$ and five free parameters: the Li I line radiation intensity A, the background B dominated by Bremsstrahlung radiation, the electronic offset Z, the instrumental function $C(\lambda)$ and the interference filter $D(\lambda)$ described in Eq. (5). Therefore, we infer these five free parameters consistent with the measured spectrum using Bayesian probability theory.

Before we do so, let us first describe basic structure of the Bayesian probability theory. What we ultimately wish to obtain is the degree of certain information being true when we are given measured data. In other words, what is the probability that a free parameter has a certain value provided the measured data? This is typically written as $p(\mathcal{I}|\mathcal{D})$ and is called *posterior* where $\mathcal{I}$ denotes the information we wish to obtain, and $\mathcal{D}$ is the measured data. Once we have this posterior probability, then we can choose $\mathcal{I}$ that maximizes the posterior, known as the *maximum a posteriori* (MAP) estimation, as the most likely information (or explanation) given the data. As the posterior probability is intrinsically an inverse problem, obtaining it is not an easy task. On the other hand, probability theory allows us to obtain the posterior as

$$\begin{aligned} p(\mathcal{I}|\mathcal{D}) &= \frac{p(\mathcal{D}|\mathcal{I})\,p(\mathcal{I})}{p(\mathcal{D})} \\ &\propto p(\mathcal{D}|\mathcal{I})\,p(\mathcal{I}), \end{aligned} \tag{16}$$

where $p(\mathcal{D}|\mathcal{I})$, $p(\mathcal{I})$ and $p(\mathcal{D})$ are *likelihood*, *prior* and *evidence*, respectively. Constructing likelihood is a forward problem which is easier than forming posterior directly (if it is even possible), and an example is Eq. (6) which tells us the probability of observing (or measuring) a certain value of a free parameter (in this example, it is A) given information (in this example, it is n_e). Prior quantifies our knowledge on information (or free parameters) before we have measured data. Evidence is typically used for a model selection and irrelevant if one is only interested in estimating free parameters; then, we have the second line in Eq. (16).

Note that as posterior is expressed in terms of probability, we naturally obtain the best estimation (using the MAP estimation) and its associated uncertainty simultaneously which are consistent with the measured data. More detailed description on Bayes theorem can be found elsewhere [18, 19].

To minimise possible confusion, we define our notations used in the following sections in Table 1 . For instance, $p(\mathbf{z}_*|\mathbf{z})$ is the probability of obtaining a column vector $\mathbf{z}_*$ given the measured column vector data $\mathbf{z}$ which is a posterior. As the JET

Expression style	Example	Meaning
Boldface	$\mathbf{y}$, $\mathbf{S}$	Column vector
Boldface with a check accent	$\check{\mathbf{K}}$, $\check{\mathbf{\Sigma}}$	Matrix
Plain	S, x	Scalar
Subscript asterisk	$\mathbf{y}_*$, S_*	Quantity to be inferred
Without subscript asterisk	$\mathbf{y}$, S	Observed (measured) or given quantity
Superscript index	$\mathbf{y}^i$, x^i	Quantity of the i^{th} channel out of the total 26 spatial positions (channels) of the JET Li-BES system
Subscript index	$\mathbf{y}_i$, x_i	Quantity in the i^{th} pixel of the CCD camera

Table 1. Notations used in Sec. 3.

Li-BES system obtains spectra from 26 different spatial positions (channels) and the CCD pixels correspond to wavelength, our data can be represented in a matrix form of $\check{\mathbf{S}}$, i.e., rows for channels and columns for CCD pixels (wavelength). Then, the signal at the i^{th} channel and j^{th} pixel is denoted as S^i_j, a measured scalar quantity.

Using these notations, our main goal of this paper is to find posterior $p\left(S^i_{j*}|S^i_j\right)$ where

$$S^i_{j*} = D^i_{j*}\left(C^i_{j*}A^i_* + B^i_*\right) + Z^i_*. \tag{17}$$

The key quantity to infer electron density n_e is A^i_* as discussed in Sec. 2.3. Of course, other free parameters are important as well since they can affect the value of A^i_*. In the following sections, we describe how these five free parameters are inferred in detail by invoking Bayesian probability theory.

3.1. Interference filter and instrumental functions

We wish to infer the i^{th} channel interference filter function $\mathbf{D}^i_*$, a column vector as it is a function of the CCD pixel (wavelength). For this purpose, we illuminate uniform and constant LED lights to the system without plasma discharges so that there is no Li I line radiation. Therefore, we have posterior $p\left(\mathbf{S}^i_*|\mathbf{S}^i\right)$ where

$$\mathbf{S}^i_* = \mathbf{D}^i_* B^i_* + Z^i_* = \mathbf{D}^i_*, \tag{18}$$

where we have set $B^i_* = 1$ and $Z^i_* = 0$. Having $Z^i_* = 0$ is supported by Fig. 4 which are interference filter functions where the *residual* offset‖ is indeed negligible. We explain why we are allowed to have $B^i_* = 1$ once we obtain $\mathbf{D}^i_*$ later. Then, Bayes formula tells us that this posterior is

$$p\left(\mathbf{D}^i_*|\mathbf{S}^i\right) \propto p\left(\mathbf{S}^i|\mathbf{D}^i_*\right) p\left(\mathbf{D}^i_*\right). \tag{19}$$

‖ This is the residual offset after $\bar{Z}_{\text{CCD}}$ is removed as discussed in Sec. 2.3.2.

Our task now simply becomes constructing likelihood and prior. Likelihood follows the Gaussian distribution similar to Eq. (6) except that we now deal with a vector quantity:

$$p\left(\mathbf{S}^i|\mathbf{D}^i_*\right) = \frac{1}{\sqrt{(2\pi)^{N_{\text{pixel}}}\left|\check{\mathbf{\Sigma}}\right|}} \exp\left[-\frac{1}{2}\left(\mathbf{S}^i - \mathbf{D}^i_*\right)^T \check{\mathbf{\Sigma}}^{-1}\left(\mathbf{S}^i - \mathbf{D}^i_*\right)\right], \quad (20)$$

where the superscript T is the usual transpose operator and N_{pixel} the total number of CCD pixels for the i^{th} channel we consider. $\check{\mathbf{\Sigma}}$ is a $N_{\text{pixel}} \times N_{\text{pixel}}$ square diagonal matrix containing variances of the measured signal at each pixel of the CCD camera as in

$$\check{\mathbf{\Sigma}} = \begin{bmatrix} \sigma_1^2 & & & & & \\ & \sigma_2^2 & & & & \\ & & \cdots & & & \\ & & & \sigma_j^2 & & \\ & & & & \cdots & \\ & & & & & \sigma^2_{N_{\text{pixel}}} \end{bmatrix}, \quad (21)$$

where $\sigma_j^2 = \sigma^2_{\text{ph},j} + \sigma^2_{\text{e},j}$ at the j^{th} pixel as Eq. (15) is used in Eq. (6). $\sigma^2_{\text{ph},j}$ and $\sigma^2_{\text{e},j}$ can be estimated as described in Sec. 2.3.2. Note that $\check{\mathbf{\Sigma}}$ is different for different channels..

Prior $p\left(\mathbf{D}^i_*\right)$ in Eq. (19) needs to be specified. Since we do not know the parametric form, i.e., analytical form, describing the i^{th} channel interference filter $\mathbf{D}^i_*$ as a function of CCD pixels (or wavelength), we utilise a non-parametric technique known as Gaussian process [16]:

$$p\left(\mathbf{D}^i_*\right) = \frac{1}{\sqrt{(2\pi)^{N_{\text{pixel}}}\left|\check{\mathbf{K}}\right|}} \exp\left[-\frac{1}{2}\left(\mathbf{D}^i_* - \mathbf{0}\right)^T \check{\mathbf{K}}^{-1}\left(\mathbf{D}^i_* - \mathbf{0}\right)\right]. \quad (22)$$

Here, $\mathbf{0}$ is a column vector whose entries are all zeros. The $N_{\text{pixel}} \times N_{\text{pixel}}$ matrix $\check{\mathbf{K}}$, which varies channel by channel, is a squared exponential covariance function with the value at the j^{th} row and k^{th} column of

$$K_{jk} = \sigma_f^2 \exp\left[-\frac{1}{2\ell^2}\left|x_j - x_k\right|^2\right] + \sigma_n^2 \delta_{jk}. \quad (23)$$

δ_{jk} is the usual Kronecker delta. $\mathbf{x}$ is a vector of the CCD pixel, thus $|x_j - x_k|$ is the pixel distance between the j^{th} and k^{th} pixels. Gaussian process contains *hyperparameters*: σ_f^2 is the signal variance, ℓ the scale length and σ_n^2 the noise variance. These hyperparameters govern the characteristic of the Gaussian process Eq. (22), and we find their values by maximizing the evidence $p\left(\mathbf{S}^i\right)$. More detailed description can be found elsewhere [15].

We now have no unknowns to find posterior Eq. (19), and Fig. 4(a) shows the comparison between the measured $\mathbf{S}^i$ and the best (MAP) estimation of inferred $\mathbf{D}^i_*$ for the channel 18. Fig. 4(b) shows the best (MAP) estimation of the filter functions for all channels of the JET Li-BES system. Note that we normalise all the filter functions to have the maximum value of one as what we need is the *shape* of the filter functions in the pixel (wavelength) domain; thus $B^i_* = 1$ in Eq. (18) is allowed. This does not

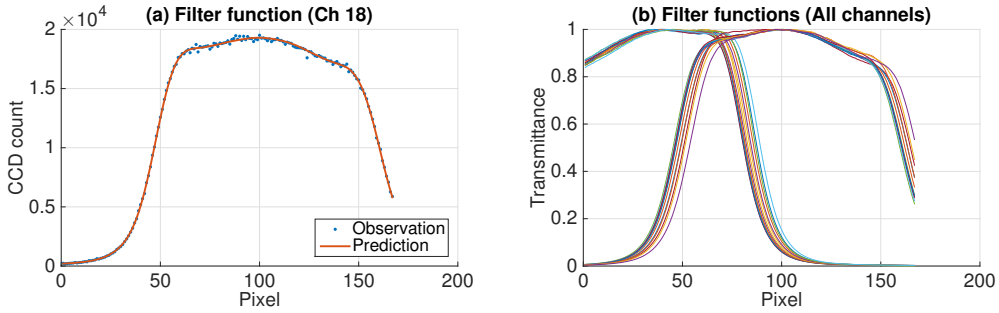

Figure 4. (a) The measured filter function (dots) and the best (MAP) estimation of the inferred filter function (red line) for the channel 18 using Bayes formula with Gaussian process prior showing a good agreement between the two. (b) Normalised inferred filter functions (MAP) for all channels shown in different colours.

create any problems because relative sensitivities among the channels are captured by the instrumental functions as relative calibration factors, while α in Eq. (11) takes care of the absolute calibration factor.

To infer the i^{th} channel instrumental function $\mathbf{C}^i_*$, we use beam-into-gas shots. During the beam-into-gas shots, neutral lithium beam atoms are injected into the tokamak filled with a neutral deuterium gas whose pressure is less than 10^{-4} mbar. Because there is no plasmas, there exists negligible amounts of Bremsstrahlung. For this case, our posterior is $p\left(\mathbf{S}^i_*|\mathbf{S}^i\right)$ with

$$\mathbf{S}^i_* = \mathbf{D}^i\mathbf{C}^i_*A^i_* + Z^i_*, \tag{24}$$

i.e., $S^i_{j*} = D^i_j C^i_{j*} A^i_* + Z^i_*$ at the j^{th} pixel, where the interference filter function $\mathbf{D}^i$ is set to be the best estimation of $p\left(\mathbf{D}^i_*|S_*\right)$ in Eq. (19); therefore, $\mathbf{D}^i$ is not to be inferred here. Furthermore, we set $A^i_* = 1$ for all channels. Due to the small deuterium pressure inside the tokamak during the beam-into-gas discharges, no indication of the beam attenuation was found in the data within their accuracy [9] resulting in no reduction of the beam density along the beam coordinate z. Therefore, the populated photons $N^{\text{pop}}_{\text{ph}}\left(z\right)$ in Eq. (8) does not vary along z resulting in the same A^i if there were no difference in T, Q, Δz, $\mathbf{D}^i$ or $\mathbf{C}^i$ in Eq. (11) for all channels. This is not the reality. By having $A^i = 1$, $\mathbf{C}^i_*$ is forced to include these effects of differences among the channels as a *relative calibration factor*. We include Z^i_* to be inferred here because it is not negligible for some channels as shown in Fig. 5.

We infer $\mathbf{C}^i_*$ and Z^i_* as done for the interference filter functions. Likelihood $p\left(\mathbf{S}^i|\mathbf{S}^i_*\right)$ with $\mathbf{S}^i_* = \mathbf{D}^i\mathbf{C}^i_* + Z^i_*$ has the same form as in Eq. (20). We let prior $p\left(\mathbf{C}^i_*\right)$ to have the form of Eq. (22) with the covariance function Eq. (23) employing a non-parametric technique. Again, the hyperparameters are set such that evidence is maximised. Prior $p\left(Z^i_*\right)$ has a form of a Gaussian distribution with a zero mean and an extremely large variance, i.e., the variance is set to 10^6 so that it is almost uniform within the plausible values of Z^i_* whose inferred value is typically a few tens. With likelihood and prior, we have posterior, and Fig. 5(a) compares the measured and inferred instrumental function (MAP) for the channel 18. Fig. 5(b) shows the inferred instrumental functions (MAP)

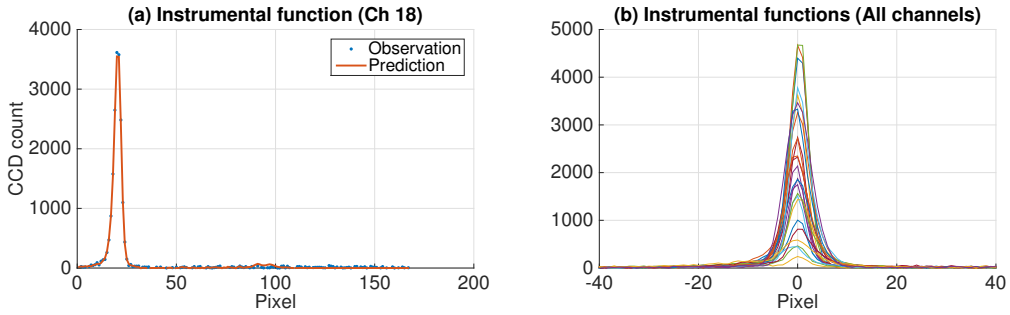

Figure 5. (a) The measured instrumental function (dots) and the best (MAP) estimation of the instrumental function (red line) for the channel 18. (b) Inferred instrumental functions (MAP) for all channels shown in different colours. Note that the instrumental functions are not normalised in order to capture the relative sensitivities, and during the beam-into-gas there is no indication of the beam attenuation.

for all channels, and the different heights, i.e., CCD counts, for the different instrumental functions mean the differences in the *relative* sensitivities. This information is used to calculate the relative calibration factors.

3.2. Line intensities

Out of five free parameters in Eq. (17), we inferred $\mathbf{D}^i_*$ and $\mathbf{C}^i_*$ from Sec. 3.1 and are left with three free parameters: A^i_*, B^i_* and Z^i_*. These parameters are what we infer using the data $\mathbf{S}^i$ measured by the JET Li-BES system by injecting the neutral lithium beam atoms into the plasmas, and A^i_* is used to infer the electron density in Sec. 3.3.

The inference is performed within the Bayesian scheme where posterior has the usual form of $p\left(\mathbf{S}^i_*|\mathbf{S}^i\right)$ with $\mathbf{S}^i_* = \mathbf{D}^i\left(\mathbf{C}^i A^i_* + B^i_*\right) + Z^i_*$. The same form of Eq. (20) is, again, used as likelihood $p\left(\mathbf{S}^i|\mathbf{S}^i_*\right)$. As we have three independent free parameters, our prior $p\left(\mathbf{S}^i_*\right)$ is

$$p\left(\mathbf{S}^i_*\right) = p\left(A^i_*, B^i_*, Z^i_*\right) = p\left(A^i_*\right) p\left(B^i_*\right) p\left(Z^i_*\right), \tag{25}$$

where all three prior probabilities are chosen to follow Gaussian distributions with the zero means and the variances of 10^6. Priors are selected as uniform as possible within the range of feasible values of A^i_*, B^i_* and Z^i_*.

These three parameters are inferred from posterior, and the comparison between the inferred quantity (MAP) and observation at 50.260 sec of the JET shot number 87861 for the channel 8 is shown in Fig. 6(a). Fig. 6(b) and (c) show the inferred profiles of Li I line intensity A^i_* and the background intensity B^i_* with their uncertainties (the shortest 95 % confidence interval), respectively. Note that the edge n_e profiles are directly inferred from the Li I line intensities, and the effective charge $Z_{\rm eff}$ profiles are possibly inferred from the background intensities since Bremsstrahlung intensities are linearly proportional to $Z_{\rm eff}$, i.e., the intensity of Bremsstrahlung radiation $I_{\rm Brem} \propto Z_{\rm eff} n_e^2 T_e^{1/2}$.

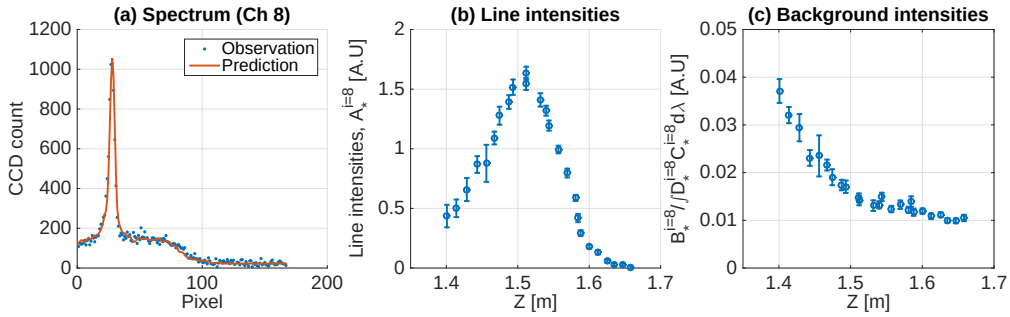

Figure 6. (a) The measured spectrum (dots) and their best (MAP) estimation at 50.260 sec of the shot number 87861 for channel 8. Inferred profiles of (b) Li I line and (c) background intensities with their associated uncertainties.

3.3. Edge electron density profiles

We now have the best (MAP) estimation of the Li I line intensities with the associated uncertainties consistent with the measured data as shown in Fig. 6(b), which we denote them as $\mathbf{A} \pm \sigma_{\mathbf{A}} = \{A^i \pm \sigma_A^i | i = 1, 2, \cdots, 25, 26\}$ where the superscript i denotes the channel number as before. Note that we take the Li I line intensity $\mathbf{A} \pm \sigma_{\mathbf{A}}$ as the given data here because it has been estimated in Sec. 3.2; therefore, this quantity has no subscript $*$. According to Eq. (11), the problem of reconstructing edge electron density profiles simply becomes calculating posterior $p\left(\mathbf{N}_{2*}\left(\mathbf{n}_{\mathbf{e}*}\right), \alpha_* | \mathbf{A}, \sigma_{\mathbf{A}}\right)$, i.e.,

$$p\left(\mathbf{N}_{2*}\left(\mathbf{n}_{\mathbf{e}*}\right), \alpha_* | \mathbf{A}, \sigma_{\mathbf{A}}\right) \propto p\left(\mathbf{A}, \sigma_{\mathbf{A}} | \mathbf{N}_{2*}\left(\mathbf{n}_{\mathbf{e}*}\right), \alpha_*\right) p\left(\mathbf{N}_{2*}\left(\mathbf{n}_{\mathbf{e}*}\right), \alpha_*\right), \quad (26)$$

where the absolute calibration factor α_* and the relative population of the first excited state $\mathbf{N}_{2*}$ which depends on the edge electron density profile $\mathbf{n}_{\mathbf{e}*}$ as in Eq. (3) are the free parameters whose values we wish to obtain. Of course, α_* is a scalar quantity, i.e., a constant for all channels, because any relative sensitivity among the different channels are captured within the instrumental functions $\mathbf{C}^i$.

Likelihood $p\left(\mathbf{A}, \sigma_{\mathbf{A}} | \mathbf{N}_{2*}\left(\mathbf{n}_{\mathbf{e}*}\right), \alpha_*\right)$ is set to follow a Gaussian distribution function as have been done for all likelihoods in this paper, and it is

$$\begin{aligned} &p\left(\mathbf{A}, \sigma_{\mathbf{A}} | \mathbf{N}_{2*}\left(\mathbf{n}_{\mathbf{e}*}\right), \alpha_*\right) \\ &= \frac{1}{\sqrt{(2\pi)^{N_{\mathrm{ch}}} \left|\check{\mathbf{\Sigma}}_A\right|}} \exp\left[-\frac{1}{2}\left(\mathbf{A} - \alpha_* \mathbf{N}_{2*}\left(\mathbf{n}_{\mathbf{e}*}\right)\right)^T \check{\mathbf{\Sigma}}_A^{-1}\left(\mathbf{A} - \alpha_* \mathbf{N}_{2*}\left(\mathbf{n}_{\mathbf{e}*}\right)\right)\right], \end{aligned} \quad (27)$$

where $N_{\mathrm{ch}} = 26$ is the total number of the channels. $\check{\mathbf{\Sigma}}_A$ is the $N_{\mathrm{ch}} \times N_{\mathrm{ch}}$ diagonal matrix with the entry of $\left(\sigma_A^i\right)^2$ at the i^{th} row and i^{th} column. We calculate $\alpha_* \mathbf{N}_{2*}\left(\mathbf{n}_{\mathbf{e}*}\right)$ using the Runge-Kutta method (RK4) with the initial condition Eq. (4).

Prior $p\left(\mathbf{N}_{2*}\left(\mathbf{n}_{\mathbf{e}*}\right), \alpha_*\right)$ is now only the unknown to obtain posterior. Because $\mathbf{N}_{2*}\left(\mathbf{n}_{\mathbf{e}*}\right)$ and α_* are independent to each other, we have $p\left(\mathbf{N}_{2*}\left(\mathbf{n}_{\mathbf{e}*}\right), \alpha_*\right) = p\left(\mathbf{N}_{2*}\left(\mathbf{n}_{\mathbf{e}*}\right)\right) p\left(\alpha_*\right)$. Due to the complete ignorance on the value of α_*, we let $p\left(\alpha_*\right)$ to be simply a uniform distribution function. $p\left(\mathbf{N}_{2*}\right)$ can be easily calculated if $p\left(\mathbf{n}_{\mathbf{e}*}\right)$ is available using Eq. (3). Furthermore, we have huge amount of edge n_e profile data

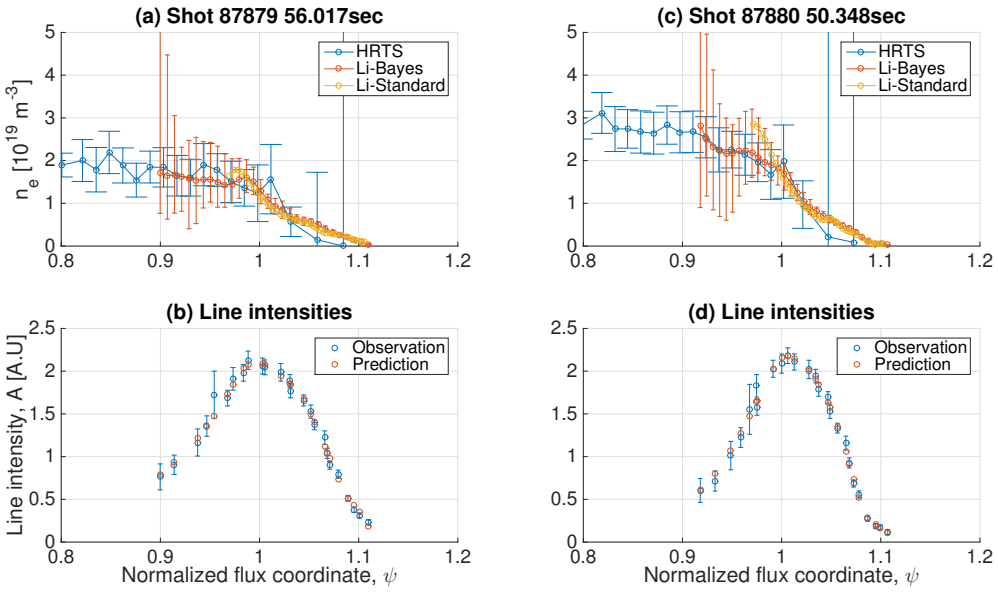

Figure 7. (a) Best (MAP) estimation of the inferred edge electron density profile (red) and the associated uncertainties which include 95% of the samples from posterior with the n_e profiles from the HRTS system (blue) and obtained using the conventional data analysis method (yellow) of the JET Li-BES system and (b) the observed Li I intensity (blue), i.e., $\mathbf{A}$ in Eq. (26), and the predicted (or inferred) intensity (red), i.e., $\alpha_* \mathbf{N}_{2*}(\mathbf{n}_{\mathbf{e}*})$ for the shot #87879 at 56.017 sec. (b) and (d) are same as (a) and (c) for the shot #87880 at 50.348 sec.

from many years of JET experiments. Based on these existing data, we construct $p(\mathbf{n}_{\mathbf{e}*})$ using Gaussian process similar to Eq. (22) where N_{pixel} is replaced by N_{ch}; and the hyperparameters σ_f and ℓ for the covariance matrix $\check{\mathbf{K}}$ are set to be 20.0 and 0.025, respectively. We note that these values for the hyperparameters are not rigorously obtained by maximising the evidence due to the requirement of too much computation time. Nevertheless, these values reasonably support the most of the existing n_e profiles from JET. Representing density profiles using Gaussian processes and its advantages can be found elsewhere [20].

Posterior of $\mathbf{N}_{2*}$ (thus, $\mathbf{n}_{\mathbf{e}*}$) and α_* is explored by Markov Chain Monte Carlo (MCMC) method, and Fig. 7(a) and (c) show the best (MAP) estimation of the inferred edge electron density profiles (red) with their associated uncertainties which cover 95% of the samples from posterior, i.e., the shortest 95% confidence interval. For the sake of comparison, n_e profiles from the HRTS system (blue) and obtained via the conventional data analysis method (yellow) of the JET Li-BES system [9, 10] are also shown in the same figures. Fig. 7(b) and (d) show the observed Li I line intensity (blue), i.e., $\mathbf{A}$ in Eq. (26), and the predicted (or inferred) intensity (red), i.e., $\alpha_* \mathbf{N}_{2*}(\mathbf{n}_{\mathbf{e}*})$, for Fig. 7(a) and (c), respectively.

It is clear from these results that we have inferred a proper absolute calibration factor α even if we have not used the singular point method [4] as the absolute value of

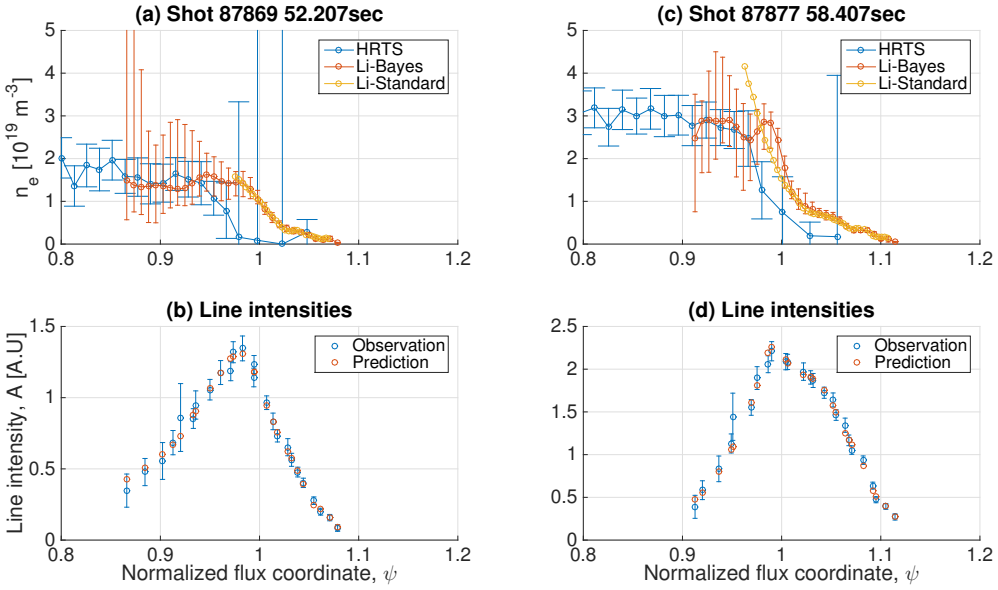

Figure 8. Same as Fig. 7 for different time and shot number which show disagreement between the Li-BES data and HRTS data.

the density profiles agree with the HRTS data. The range of the inferred profile has been extended to the full observation range which was not possible with the conventional data analysis method. We stress that we have not used a separate background measurement via Li neutral beam modulations because our method is capable of providing intensities of Li I line radiation and background simultaneously. Finally, we also have not used a monotonic profile assumption.

Fig. 8 shows the edge electron density profiles we obtain sometimes which are different from those obtained by the HRTS system in JET. We note that such a discrepancy cannot be explained by mis-inference of the absolute calibration factor. If the absolute calibration factor were the cause, then we would have neither i) the agreement between our proposed method (red) and the conventional method (yellow) based on the JET Li-BES data, nor ii) the observed *shift* of the profiles in the radial direction with respect to the HRTS data (blue). Calibration of the spatial position for the JET Li-BES may be questioned. However, this calibration is performed with relatively high reliability [9]. We do suspect that it may have been caused due to the EFIT reconstruction. The JET Li-BES system injects the neutral Li beam vertically from the top of the JET at the major radius $R = 3.25$ m and covering the vertical position $Z = 1.67 \sim 1.40$ m approximately; whereas the HRTS system observes electron density along the laser penetrating horizontally at the midplane ($R = 2.9 \sim 3.9$ m and $Z = 0.06 \sim 0.11$ m). EFIT reconstruction may well have inaccurate flux coordinate at the top of the plasmas compared to the midplane. We leave further investigation of this issue as a future work.

An astute reader may realize that uncertainties of the estimated electron densities in

the inner region is larger than those of the outer region. This result cannot be explained solely by the detected photon intensities as attested by Fig. 7 and Fig. 8. Furthermore, this trend of larger uncertainties in the inner region is also observed in ASDEX-U as well [7, 21]. Here, we provide two qualitative reasons to explain this trend. As shown in Fig. 1, the relative population of the first excited state N_2 becomes less sensitive to the change of n_e as it increases. Typically, n_e is larger in the inner region than the outer region, therefore the similar level of uncertainty in N_2 corresponds to a larger uncertainty of n_e in the inner region. In addition, the neutral Li beam attenuation as it penetrates into the plasmas can cause this trend of increasing uncertainties. Consider two separate measurements of the absolute number of the first excited state 200 ± 20 where the total number of neutral beam atoms is 500 in one case and 1000 in another case. Then, the relative population N_2 is $(200 \pm 20)/500 = 0.4 \pm 0.04$ for the former case and $(200 \pm 20)/1000 = 0.2 \pm 0.02$ for the latter case. It is evident that the former case has the larger uncertainty than the latter case even if the absolute number of the first excited state are the same for both cases. Therefore, the beam attenuation, i.e., decrease of the total number of beam atoms, can cause the larger uncertainty of n_e in the inner region. We leave the quantitative studies on our rationale as the future work. Finally, we note that there can be additional effects from the uncertainties of the absolute calibration factor [4, 8].

4. Conclusion

In this paper, we have thoroughly presented our newly developed data analysis scheme to obtain edge electron density profiles based on the measured JET Li-BES data. Our proposed Bayesian electron density inference using Gaussian process is implemented in Minerva platform. Our scheme includes uncertainties due to photon statistics and electrical fluctuations estimated from the measured data. Instrumental effects such as the interference filter function and instrumental function are inferred from the separate measurements with Gaussian process prior where their hyperparameters are selected by maximising evidence. The Li I line and background intensities are simultaneously inferred as well as their associated uncertainties, thereby eliminating extra effort of measuring background intensity via Li neutral beam modulations.

This Li I line intensity is directly used to infer the edge electron density profile where the predicted (or inferred) line intensities are calculated based on the multi-state model using Runge-Kutta method. Electron density profiles whose prior is set by Gaussian process based on the pre-existing electron density profiles from JET are obtained via the Markov Chain Monte Carlo (MCMC) method from posterior and its best, i.e., maximum a posterior (MAP), estimation. The associated uncertainties are also simultaneously obtained consistent with the measured data. The results have been compared with the electron density profiles from the high resolution Thomson scattering (HRTS), and they agree within their accuracy.

Our proposed scheme has at least following major advantages: it provides i) all

possible electron density profiles and their uncertainties consistent with the data, ii) edge electron density profiles on the full observation range and iii) the automatic absolute calibration factor without using the singular point of the electron density profile, thereby removing both the necessity of preprocessing the data such as smoothing of the data to find the singular point position and the inner boundary assumption which is required when the singular point does not exist in a conventional method. Furthermore, constructing prior for the electron density profile based on Gaussian process has allowed us not to use the assumption of non-monotonic profile which is important as the profiles may well be non-monotonic in reality. Finally, our method does not require performing Li neutral beam modulations.

Acknowledgement

This research was supported by National R&D Program through the National Research Foundation of Korea (NRF) funded by the Ministry of Science, ICT (grant number NRF-2014M1A7A1A01029835), and the KUSTAR-KAIST Institute, KAIST, Korea. This work has been carried out within the framework of the EUROfusion Consortium and has received funding from the Euratom research and training programme 2014-2018 under grant agreement No 633053. The views and opinions expressed herein do not necessarily reflect those of the European Commission.

References

[1] Zohm H 1996 *Plasma Phys. Controlled Fusion* **38** 105

[2] Wagner F, Fussmann G, Grave T, Keilhacker M, Kornherr M, Lackner K, McCormick K, Müller E R, Stäbler A, Becker G, Bernhardi K, Ditte U, Eberhagen A, Gehre O, Gernhardt J, Gierke G v, Glock E, Gruber O, Haas G, Hesse M, Janeschitz G, Karger F, Kissel S, Klüber O, Lisitano G, Mayer H M, Meisel D, Mertens V, Murmann H, Poschenrieder W, Rapp H, Röhr H, Ryter F, Schneider F, Siller G, Smeulders P, Söldner F, Speth E, Steuer K H, Szymanski Z and Vollmer O 1984 *Phys. Rev. Lett.* **53** 1453

[3] Carreras B A 1997 *IEEE Trans. Plasma Sci.* **25** 1281

[4] Schweinzer J, Wolfrum E, Aumayr F, Pockl M, Winter H, Schorn R P, Hintz E and Unterreiter A 1992 *Plasma Phys. Controlled Fusion* **34** 1173

[5] Wolfrum E, Aumayr F, Wutte D, Winter H P, Hintz E, Rusbüldt D and Schorn R P 1993 *Rev. Sci. Instrum.* **64** 2285–2292

[6] McCormick K, Fiedler S, Kocsis G, Schweinzer J and Zoletnik S 1997 *Fusion Eng. Des.* **34–35** 125

[7] Fischer R, Wolfrum E, Schweinzer J and the ASDEX Upgrade Team 2008 *Plasma Phys. Controlled Fusion* **50** 085009

[8] Pietrzyk Z A, Breger P and Summers D D R 1993 *Plasma Phys. Controlled Fusion* **35** 1725

[9] Brix M, Dodt D, Korotkov A, Morgan P, Dunai D, Fischer R, Meigs A, Nedzelskiy I S, Schweinzer J, Vince J, Zoletnik S and Contributors J E 2010 *Rev. Sci. Instrum.* **81** 10D733

[10] Brix M, Dodt D, Dunai D, Lupelli I, Marsen S, Melson T F, Meszaros B, Morgan P, Petravich G, Refy D I, Silva C, Stamp M, Szabolics T, Zastrow K D, Zoletnik S and Contributors J E 2012 *Rev. Sci. Instrum.* **83** 10D533

[11] Schorn R, Hintz E, Rusbüldt D, Aumayr F, Schneider M, Unterreiter E and Winter H 1991 *Appl. Phys. B* **52** 71

[12] Svensson J and Werner A 2007 Large scale bayesian data analysis for nuclear fusion experiments *Intelligent Signal Processing, 2007. WISP 2007. IEEE International Symposium on* pp 1–6
[13] Open-adas URL `http://open.adas.ac.uk`
[14] Schweinzer J, Brandenburg R, Bray I, Hoekstra R, Aumayr F, Janev R and Winter H 1999 *Atomic Data and Nuclear Data Tables* **72** 239
[15] Kwak S, Svensson J, Brix M, Ghim Y c and JET Contributors 2016 *Rev. Sci. Instrum.* **87** 023501
[16] Rasmussen C E and Williams C K I 2006 *Gaussian Processes for Machine Learning* (MIT Press)
[17] Pasqualotto R, Nielsen P, Gowers C, Beurskens M, Kempenaars M, Carlstrom T, Johnson D and Contributors J E 2004 *Rev. Sci. Instrum.* **75** 3891–3893
[18] Sivia D 1996 *Data Analysis: A Bayesian Tutorial* Oxford science publications (Clarendon Press)
[19] von der Linden W, Dose V and von Toussaint U 2014 *Bayesian Probability Theory: Applications in the Physical Sciences* (Cambridge)
[20] Chilenski M, Greenwald M, Marzouk Y, Howard N, White A, Rice J and Walk J 2015 *Nucl. Fusion* **55** 023012
[21] Willensdorfer M, Birkenmeier G, Fischer R, Laggner F M, Wolfrum E, Veres G, Aumayr F, Carralero D, Guimaris L, Kurzan B and the ASDEX Upgrade Team 2014 *Plasma Physics and Controlled Fusion* **56** 025008 URL `http://stacks.iop.org/0741-3335/56/i=2/a=025008`